JACS
JOURNAL OF THE AMERICAN CHEMICAL SOCIETY
Article
pubs.acs.org/JACS

Tailor-Made Highly Luminescent and Ambipolar Transporting Organic Mixed Stacked Charge-Transfer Crystals: An Isometric Donor–Acceptor Approach

Sang Kyu Park,[†] Shinto Varghese,[‡] Jong H. Kim,[†] Seong-Jun Yoon,[†] Oh Kyu Kwon,[†] Byeong-Kwan An,[§] Johannes Gierschner,*[,‡] and Soo Young Park*[,†]

[†]Center for Suprameolcular Optoelectronic Materials and WCU Hybrid Materials Program, Department of Materials Science and Engineering, Seoul National University, 1 Gwanak-ro, Gwanak-gu, Seoul 151-744, Korea

[‡]Madrid Institute for Advanced Studies, IMDEA Nanoscience, Calle Faraday 9, Ciudad Universitaria de Cantoblanco, 28049 Madrid, Spain

[§]Department of Chemistry, The Catholic University of Korea, Bucheon-si, Geyonggi-do 420-753, Korea

Supporting Information

ABSTRACT: We have rationally designed a densely packed 1:1 donor–acceptor (**D**–**A**) cocrystal system comprising two isometric distyrylbenzene- and dicyanodistyrylbenzene-based molecules, forming regular one-dimensional mixed stacks. The crystal exhibits strongly red-shifted, bright photoluminescence originating from an intermolecular charge-transfer state. The peculiar electronic situation gives rise to high and ambipolar p-/n-type field-effect mobility up to 6.7×10^{-3} and 6.7×10^{-2} $cm^2 V^{-1} s^{-1}$, respectively, as observed in single-crystalline OFETs prepared via solvent vapor annealing process. The unique combination of favorable electric and optical properties arising from an appropriate design concept of isometric **D**–**A** cocrystal has been demonstrated as a promising candidate for next generation (opto-)electronic materials.

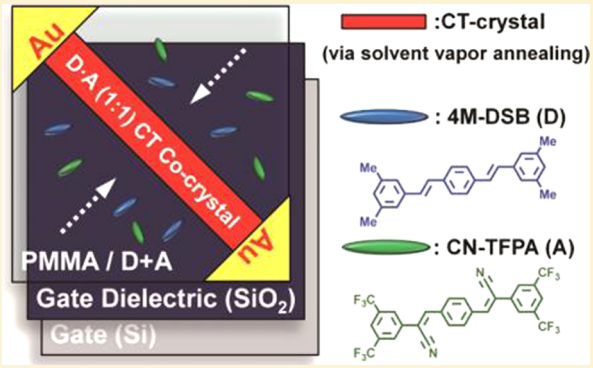

1. INTRODUCTION

Over several decades, much interest has been focused on organic solid-state semiconducting materials, due to their potential use in various (opto-)electronic device applications, such as organic light emitting diode (OLED),[1] organic photovoltaic devices (OPV),[2] and organic field-effect transistors (OFETs).[3] Among them, ambipolar charge carrier transport in organic semiconductors[4] have raised much attention as potential alternatives for complementary metal oxide semiconductors (CMOS) in high-performing memory devices.[5] However in the majority of the cases, organic semiconductors show only unipolar charge transport mainly due to the unbalanced electronic coupling of the frontier molecular orbitals (FMOs).[6] Therefore, several different approaches have been explored to realize ambipolar organic materials, such as bridged electron donor–acceptor (**D**–**A**) moieties,[7] p-/n-channel semiconductor blends or bilayers,[8,9] and cocrystallization or coassembly of **D** and **A** molecules.[10,11] In some appropriate cases, such **D**–**A** structures form charge-transfer (CT) complexes, opening a new prospect for realizing next generation (opto-)electronic applications.[12] To this end, many supramolecular chemists have devoted their efforts to find predictable **D**–**A** stacking structures with prominent CT interaction from the extensive libraries of organic material systems.[13] In spite of such efforts, (opto-)electronic application of such **D**–**A** cocrystal systems has rarely been achieved,[12] especially for ambipolar OFETs application.

Organic CT complexes can exhibit two different types of binary molecular stacking structures, being segregated or mixed stacks. Most in-depth investigations so far have been focused on the former cases due to their unconventional metallic (super)conductivities.[14] Very recently, mixed stacked **D**–**A** CT complexes have also been reexamined theoretically and experimentally aiming at their promising features of ferroelectricity[15] and ambipolar semiconductivity.[11,16] The electronic properties of the CT structures are mainly driven by the FMO offsets of **D** and **A** as well as their specific molecular arrangement. Thus, careful selection of **D**/**A** pair with appropriate FMOs is necessary to achieve efficient CT cocrystal system. Up to now, only limited numbers of such ambipolar binary CT cocrystals were realized, all being based on bis(ethylenedithio)- (BEDT) or dibenzo- (DB) substituted tetrathiafulvalene (TTF) as donor and (fluorinated) tetracyanoquinodimethane (F_2)TCNQ or organometallic and ionic counter parts as acceptor ($Cu[N(CN)_2]Br$, I).[11] Mixed stacked BEDT-TTF–F_2TCNQ exhibits distinct ambipolar charge transport only at low temperatures (2–60 K, metallic transport

Received: December 13, 2012

   dx.doi.org/10.1021/ja312197b | J. Am. Chem. Soc. XXXX, XXX, XXX–XXX

>10 K) with drain voltage-dependent mobilities of about 10^{-3} cm^2 V^{-1} s^{-1} for holes and electrons (μ_h/μ_e: ~1.5).[11b] Mixed stacked DBTTF−TCNQ (prepared by cosublimation) exhibited ambipolar behavior only when specific Fermi-level tuned electrodes were used.[11c,d] On the other hand, organic superconducting materials, such as layer-structured κ-(BEDT-TTF)$_2$Cu[N(CN)$_2$]Br[11e,f] and α-(BEDT-TTF)$_2$I$_3$[11g] (formed by electrochemical process) crystals, exhibited negative pressure induced phase transition (Mott insulating or charge ordered states, respectively) when placed on SiO_2/Si substrate at low temperature, which resulted in mainly n-type field-effect transport and also weak ambipolarity depending on surface states of crystal samples. It has been reported that the segregated stacked BEDT-TTF−TCNQ (formed by solution casting) exhibited balanced ambipolar field-effect mobility ~10^{-2} cm^2 V^{-1} s^{-1}, even at room temperature,[11h] while metal-like behavior was observed in the electron accumulation mode above 240 K. Very recently, remarkable and promising electronic properties of mixed stacked **D**−**A** CT crystals were theoretically predicted via quantum chemical calculations by Brédas and co-workers,[16] stressing the significance of super-exchange along the stacking direction.

Unfortunately, however, ambipolar transporting CT crystals other than TTF−TCNQ based systems (the latter normally exhibit ambipolarity at low temperature) have rarely been demonstrated. While various π-conjugated **D**−**A** CT supramolecular structures have been investigated aiming at the (opto-)electronics device applications, only few of them exhibited ambipolarity, but of rather limited performance.[12c] Therefore, it would be of great impact to demonstrate high-performance ambipolar CT cocrystals at this moment, even better if combined with bright luminescence, which might pave the way to advanced optoelectronic devices. Such alternative concepts require however tailor-made and energetically fine-tuned **D**/**A** pairs. In the past we and others have demonstrated that dicyanodistyrylbenzene (DCS) represent a class of molecules which are electronically significantly stabilized compared to the parent distyrylbenzene counterparts (DSB)[17] and at the same time offer a versatile route to realize multifunctional, color variable, and brightly luminescent single crystals.[18] Thus, a combination of DSB/DCS derivatives as **D**/**A** pairs could be considered ideal *a priori*, especially since the similar chemical structure and size of **D** and **A** (i.e., isometric approach) should promote facile and regular cocrystallization.[19,20] We thus designed a single-crystalline binary molecular cocrystal system comprising two isometric DSB- and DCS-based donor (4M-DSB, Figure 1) and acceptor (CN-TFPA,

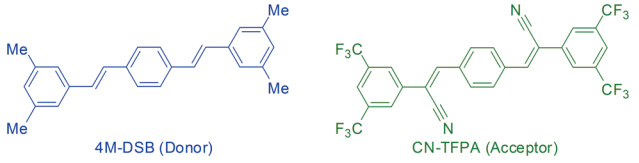

Figure 1. Chemical structures of 4M-DSB (**D**) and CN-TFPA (**A**).

Figure 1),[21] with appropriately tuned FMOs of the **D** and **A** molecules, to demonstrate unconventional bright emission together with outstanding ambipolar charge transport. As will be shown, the particular (opto-)electronic features of the newly designed **D**−**A** system are generated by a unique combination of the molecular electronic properties and the one-dimensional (1D) densely packed supramolecular arrangement driven by secondary bonding interactions. It should be noted that this design concept of isometric **D**/**A** pairs is conceptually different and advanced compared to the recently reported strategy of "lock arm supramolecular ordering" (LASO),[15] since the latter requires integrating an additional supramolecular self-assembly motif to the **D** and **A** units. Due to the remarkable structural characteristics of DCS derivatives (i.e., "twist elasticity"),[18a] single-crystalline OFETs (SC-OFETs) of the **D**−**A** cocrystal could be easily prepared by solvent vapor annealing (SVA) from solid-solution type spin-coated film.[5b,22] An in-depth structural, electrical, spectroscopic, and theoretical study allowed for a full exploration of all relevant structure−property relationships in this unique class of ambipolar CT cocrystal systems.

2. RESULTS AND DISCUSSIONS

2.1. Molecular Design. 4M-DSB (**D**) and CN-TFPA (**A**) were synthesized and characterized according to the procedures shown in the Experimental Section and Supporting Information (SI). The substitution pattern of electron-donating (CH_3) and electron-withdrawing (CF_3) groups was determined so that: (i) the luminescence is bright and in the visible; (ii) the solubility is sufficiently large by using the moderately small DSB backbone with multiple **D** or **A** substituents; (iii) dense packing is promoted by avoiding long or bulky substituents; (iv) the structural differences of **D** and **A** are as small as possible to favor mixed stacking; (v) the substituents of **D** (H, CH_3) and **A** (CN; CF_3) are complementary to promote alternating π-stacking and extend H-bonding; and (vi) the MO offset of **D** and **A** is maximized. The latter was effectively achieved by employing both CN and CF_3 functionalities in **A**, which significantly lowered the FMOs against those in **D**. Indeed, density functional theory (DFT, for details see Experimental Section) calculations suggest stabilization of **A** by 1.6 eV (1.7 eV) for the highest(lowest) (un)occupied MOs, HOMO (LUMO), see Table S1, in qualitative agreement with our experimental results (see SI). Accordingly, the electron affinity of **A** (EA_{calc} = 3.8 eV) is large enough to provide a strong driving force for a direct CT from **D** (ionization potential IP_{calc} = 5.2 eV) to **A** and to promote ambipolar charge carrier transport when composing a **D**−**A** (1:1 stoichiometric) mixed stacked CT cocrystal.

As a convenient method of realizing solid-state CT structures from the **D** and **A** molecules, we prepared nanoparticle (NP) suspensions from a 1:1 binary mixture solution of **D** and **A** in tetrahydrofurane (THF) through reprecipitation into water according to the method reported earlier by us (see Experimental Section).[23] Uniform and stable NP suspension was obtained, whose absorption and photoluminescence (PL) spectra were significantly different from those of the pure **D** or **A** NP suspensions, as shown in Figure 2c. In contrast to the rather small changes in the dilute solution system (Figure 2a), spectral changes due to the CT interaction and stacking are very prominent in the NP states. According to the strong CT interaction, new red-shifted absorption bands of moderate strength (533, 495 nm) coupled with intense orange PL (570 nm) strongly bathochromically shifted against those of **D** and **A** were newly observed in the **D**−**A** NPs. Based on such promising CT interaction in NPs, we grew high-quality bright emissive, dark-orange **D**−**A** (1:1) binary single crystals with a strongly elongated hexagonal shape, see Figure 3a.

2.2. Solid State Structure. X-ray analysis of the **D**−**A** CT cocrystal confirmed the 1:1 stoichiometry within a monoclinic

dx.doi.org/10.1021/ja312197b | J. Am. Chem. Soc. XXXX, XXX, XXX−XXX

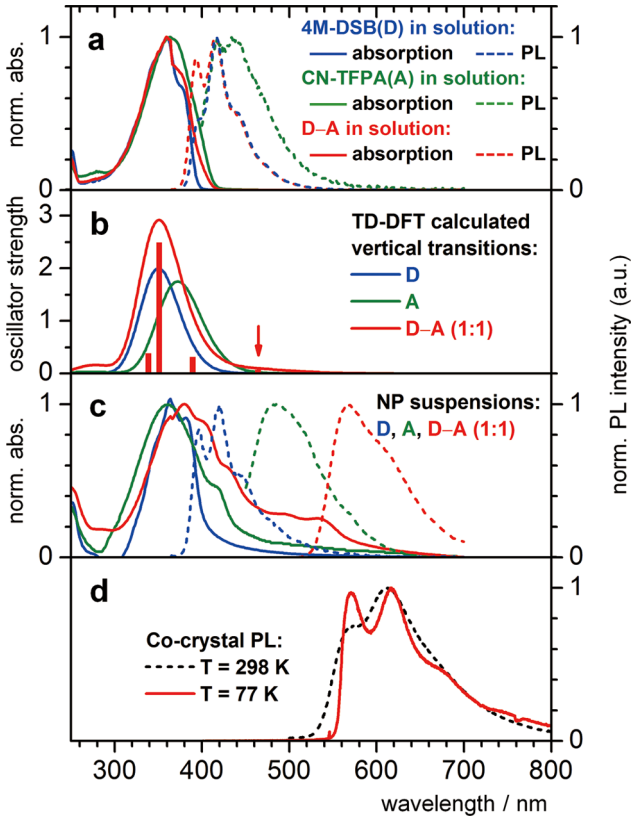

Figure 2. (a) Normalized UV–vis absorption and PL spectra of 4M-DSB (**D**), CN-TFPA (**A**), and **D** + **A** mixture in THF solution (5×10^{-6} M). (b) Calculated vertical electronic transition energies of **D**, **A**, and a **D**–**A** (1:1) dimer (broadened by a Gaussian); for **D**–**A**, transitions are also indicated as bars. (c) Normalized UV–vis absorption and PL spectra of **D**, **A**, and **D**–**A** (1:1) NP suspensions in THF:water (1:9, v:v). (d) PL spectra of the **D**–**A** (1:1) CT cocrystal at rt and 77 K with minimized reabsorption.

system, space group $P2(1)/c$, see Figure 3. The crystal consists of regular 1D mixed **D**–**A**–**D**–**A** stacks with intermolecular distances of ~3.36 Å (Figure 3d and S1) along the *b*-axis, attributed to the significant CT and subsequent Coulombic interaction between the **D** and **A** molecules, which automatically fulfilled positional locking unlike the recently reported LASO concept.[15] The molecules are practically planar in the **D**–**A** CT cocrystal (Figure S2), consistent with the "twist elasticity behavior"[18a] of the *β*-cyano-functionalized **A** molecules, which are further driven by intermolecular H-bonding (Figure S3). For a **D**–**A** pair, the electronic offset of the FMOs gives rise to a static dipole moment (SDM) of 1.22 D as calculated at the DFT(CAM-B3LYP) level of theory. The SDM of the **D**–**A** pair points in a 45° angle against the long axis of the molecules, thus oriented exactly along the crystallographic *b*-axis, as shown in Figure S4; therefore, in view of ensuring electroneutrality in the crystalline state, 90° tilt between neighboring **D**–**A**–**D**–**A** stacks is well rationalized (Figure 3b), of which the driving force is the enthalpy gain to promote dense packing. This interstack arrangement is further assisted by considerable intermolecular H-bonding interactions (–N···HC–) along the *c*-axis, similar to the molecular stacking features in the pure **A** crystal, see Figure S5.[21] This hinge-like arrangement of adjacent stacks minimizes the electronic interactions between neighboring stacks and gives rise to strongly anisotropic quasi-1D electronic characteristics of the densely packed planar **D**–**A**–**D**–**A** stacks, which is considered favorable for both p-/n-type charge transport.

2.3. Electronic and Optical Properties. The consequences of the close *π*-stacked **D**–**A** arrangements on the electronic and optical properties are conveniently and reliably elucidated by DFT calculations, by using the experimental molecular coordinates obtained from the X-ray structure analysis, see Figure 4a. It was found that the HOMO and LUMO of the stacks are totally localized on **D** and **A** moieties, respectively, as implied by the large MO offset between the designed molecules. Other MOs adjacent to the frontier orbitals, however, showed some MO delocalization with rather strong asymmetries.

The lowest electronic transition ($S_0 \rightarrow S_1$) arises mainly from a HOMO→LUMO excitation (Table S2) and thus gives a significant red-shift against the absorption of **A** (Figure 2b,c). Due to the pronounced localized character of the FMOs, the transition reveals a strong CT character as visualized by the electron–hole wave function plot in Figure S6.[19] Due to the strong CT character of the electronic transition, the transition dipole moment (TDM; with oscillator strength of 0.07) is oriented fairly along the direction of the SDM (Figure 4a), i.e., in the *b*-direction of the crystal. The energy of the transition (2.67 eV; 464 nm) agrees quite well with experiment, assuming that the low-lying peaks at 532 nm (2.32 eV) and 494 nm (2.51 eV) of the experimental spectrum (Figure 2c) represent apparent vibronics of S_1, so that the vertical transition might be around 2.5 eV. The observed band found at 428 nm (2.89 eV) should then correspond to S_2, calculated at 3.19 eV (389 nm). The main absorption band (experimentally observed at 360 nm; 3.44 eV, see Figure 2c) is assigned to the $S_0 \rightarrow S_3$ transition, calculated at 3.53 eV (351 nm). This transition of the **D**–**A** (1:1) CT cocrystal is described mainly by a HOMO→LUMO+1 excitation (Table S2), thus essentially generated by the frontier orbitals of **D**; hence, the energetic position of $S_0 \rightarrow S_3$ as well as the orientation of the TDM agree well with the $S_0 \rightarrow S_1$ transition of **D**, as indeed observed in Figure 2c.

The bright emission (PL quantum yield $\Phi_{PL} = 0.31$) and the rather well-structured PL spectrum of the **D**–**A** (1:1) CT cocrystal (which becomes especially obvious at low temperatures, see Figure 2d) might be a surprise at a first glance, since systems with significant CT character mostly show unstructured exciplex-like emissions of low intensity. We attribute the high PL efficiency of the **D**–**A** (1:1) CT cocrystal to the non-negligible oscillator strength of the S_1 state, as discussed above, and also to the low nonradiative decay often found in single crystals,[24] which is most likely due to the low trapping probability of the originally formed CT exciton. With respect to the well-resolved vibronics (which can be correlated to the respective Raman modes, see Figure S7), it is to be reminded that the decisive factor for vibronic coupling is the extent by which the normal coordinates of a considered vibration coincide with the geometrical change upon electronic de/excitation. Hence, excimer- or exciplex-like PL spectra with strongly red-shifted, unstructured features in binary CT compounds are mainly obtained, when there is a significant change in the intermolecular separation during electronic de/excitation.[25] This change is suggested to be small in the present **D**–**A** (1:1) CT cocrystal case attributed to the localized nature of the FMOs. Due to this strong localization, a pronounced change in the intermolecular coordinate upon electronic de/excitation is not expected; therefore, intermolecular modes

dx.doi.org/10.1021/ja312197b | J. Am. Chem. Soc. XXXX, XXX, XXX–XXX

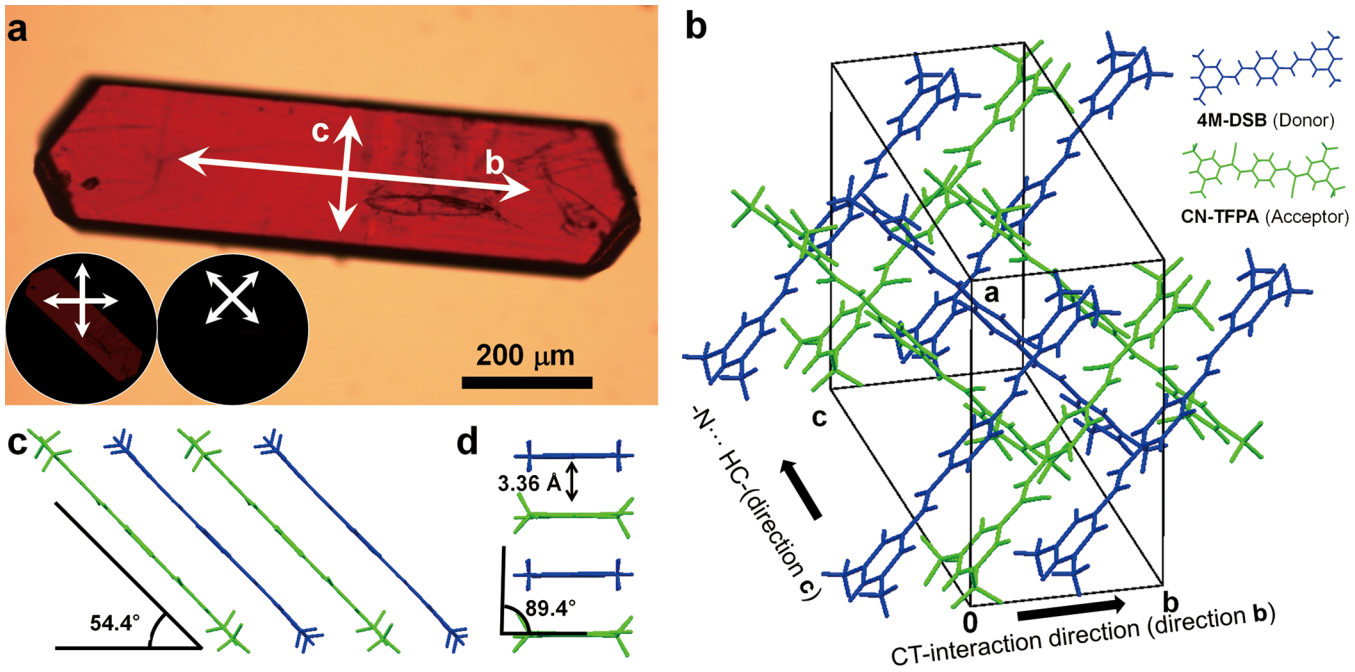

Figure 3. (a) Optical microscope image of **D**−**A** (1:1) CT cocrystal under ambient light irradiation (insets: images under ±45° rotating polarizer). (b) Single-crystal XRD structure of the **D**−**A** (1:1) CT cocrystal; blue molecule: **D**, green molecule: **A**. (c) Counter pitch angle (90° − pitch angle), and (d) counter roll angle (90° − roll angle) and π−π distance (interlayer distance) measured from single-crystal XRD results.

should have a minor influence in the vibronic structure, thus mimicking single molecular vibronics, as is apparently the case shown in Figure 2.

2.4. Charge-Transport Properties. The exclusive localization of the FMOs, as discussed above, is in fact an important prerequisite for favorable ambipolar charge transport. To estimate the potential of the binary CT cocrystal for electronics applications, we have calculated the transfer integrals for both hole and electron (t_h, t_e) along the stacking direction (i.e., *b*-axis, **D**−**A**−**D**−**A**) based on single-crystal XRD analysis, as shown in Figure 4b. The transfer integral values are known to be strongly governed by the degree of orbital overlap and to affect the effective mass of the charge carrier.[26] Following the method of Zhu et al,[16] we calculated t_h and t_e from the MO differences in **D**−**A**−**D** and **A**−**D**−**A** stacks (Figure 4b), giving t_h = 0.034 eV and t_e = 0.039 eV. The calculated values point to effective superexchange along the π-stacking direction,[16] suggesting efficient and well-balanced ambipolar charge mobility, which supports the strategy of our CT stack design concept. Since the mobility scales with t^2, the μ_e is suggested to be 30% higher than μ_h within the frame of this rather simplistic computational model.

Based on these promising results, we have carried out electrical measurements for the bottom-gate and Au top-contact SC-OFETs, see Figure 5. For this, we have employed an efficient and simple solution process, SVA,[5b,22] which we use here to grow **D**−**A** (1:1) CT cocrystals based on a ternary solid−solution type spin-coated film (composed of **D**, **A** and poly(methylmethacrylate), PMMA, as insulating polymer binding material, see Experimental Section). Here, by exposing the spin-coated blended layer to organic solvent vapor (e.g., dichloromethane, DCM), high-quality **D**−**A** (1:1) mixed stacked single crystals could be fabricated on the surface of a PMMA film, as shown in Figure 5c. Owing to the well-established advantages of introducing a polymer insulating layer, such as surface trap-site coverage and improvement of device operation stability, the SVA method allows for a precise evaluation of the charge transporting characteristics in solution-grown defect-free single crystals. The red emissive characteristics of the SVA-grown crystals (Figure 5c) are inherent to the **D**−**A** binary CT cocrystals, as described above, and exclude the possibility of mixing separate **D** and **A** crystals.

As shown in Figure 5a,b, transfer and output characteristics of **D**−**A** (1:1) SC-OFET were measured in both hole-/electron-enhancement mode at ambient temperature. The V-shape transfer curves clearly indicate the transition from ambipolar to unipolar transport with increasing V_G in both hole-/electron-enhancement mode (see Figure 5a). In addition, diode-like behaviors are apparent at low V_G regimes due to the increased injection of the opposite charge carriers; however, saturation characteristics for unipolar carrier at high V_G regimes are clearly seen in the output curves (see Figure 5b).[27] Measurements along the long crystal axis gave hole and electron mobilities up to 6.7×10^{-3} cm^2 V^{-1} s^{-1} (avg. 4.3×10^{-3} cm^2 V^{-1} s^{-1}) and 6.7×10^{-2} cm^2 V^{-1} s^{-1} (avg. 5.4×10^{-2} cm^2 V^{-1} s^{-1}), respectively, for which the capacitance values of SiO_2/PMMA layer were separately measured and used, see Figure S8. Although the experimental ambipolar character ($\mu_e/\mu_h \sim 12.6$) is somewhat less balanced compared to the theoretical predictions ($\mu_e/\mu_h \sim 1.3$), the overall good charge-transport characteristics both for p/n-channel transport strongly support our strategy to design ambipolar **D**−**A** CT cocrystals which is ascribed to the superexchange nature along the stacking direction. As one can expect, the currently measured ambipolar mobility (μ_h up to 6.7×10^{-3} cm^2 V^{-1} s^{-1} and μ_e up to 6.7×10^{-2} cm^2 V^{-1} s^{-1}) in this work is rather moderate compared to the large n-channel mobility of pure **A** crystal (5.5×10^{-1} cm^2 V^{-1} s^{-1}) in good agreement with the calculated transfer integral values of **D**−**A** mixed stack (t_h = 0.034 eV and t_e = 0.039 eV) and pure **A** arrangement (t_e = 0.079 eV);[21] however it is still good and well-balanced, due to the fact that the isometric **D**/**A** pairs with rationally designed

dx.doi.org/10.1021/ja312197b | J. Am. Chem. Soc. XXXX, XXX, XXX−XXX

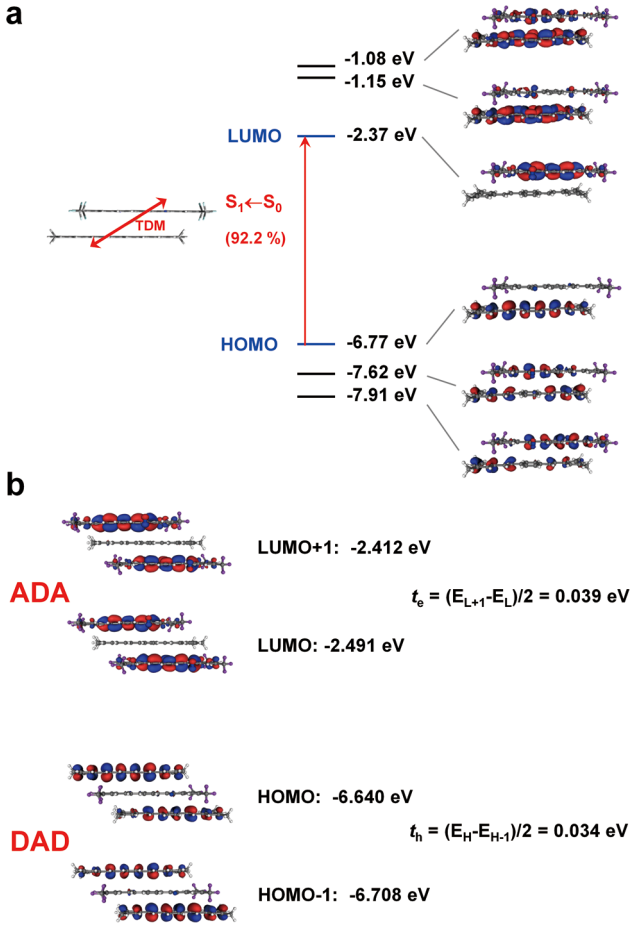

Figure 4. (a) MO diagram for the **D**−**A** (1:1) system as calculated by DFT(CAM-B3LYP); the main CI contribution for the $S_1 \leftarrow S_0$ transition is indicated; the orientation of the respective TDM is depicted on the left. (b) DFT calculated transfer integrals for electrons (t_e) and holes (t_h) along the *b*-axis based on the energy-splitting method.[16]

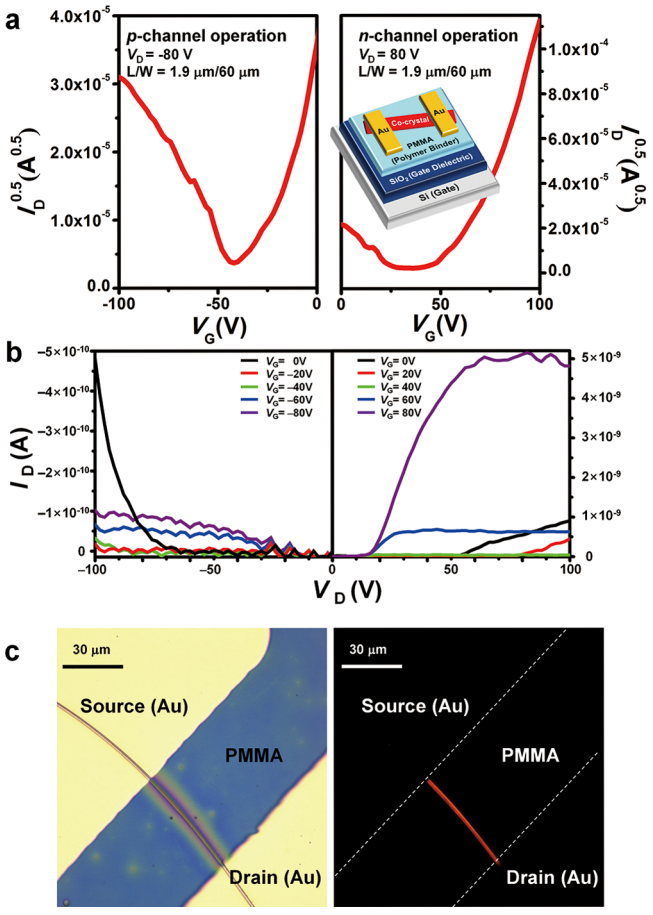

Figure 5. (a) Transfer and (b) output characteristics of the single-crystal OFET, fabricated by SVA. I_D, V_D, V_G, and L/W indicate drain current, drain voltage, gate voltage and length-to-width ratio of the active channel cocrystal. Inset: schematic drawing of the device structure. (c) Optical microscope image of a single-crystal OFET (left: under ambient light, right: under UV).

substituents on them actually gave rise to the most tight **D**−**A**−**D**−**A** packing, revealing high counter role and counter pitch angles (89.4° and 54.4°, respectively) with close π-stacking distance (3.36 Å), to ensure excellent ambipolar transporting characteristics, see Figure 3c,d.

In order to prove whether the favored charge transport direction (along the long crystal axis) indeed coincides with the stacking direction (*b*-axis), we investigated the absolute orientation of the molecules with respect to the crystal facets. Combined out-of-plane XRD measurements (Figure S9a) and height profile from atomic force microscopy (AFM) (Figure S9b) evidence that the crystal facet coincides with the (1 0 0) plane. To determine the orientation of the stacking direction (*b*-axis) against the long crystal axis, we carried out polarized PL experiments (see Experimental Section and Figure S10 for the details) since the TDM of the emitting dipole is pointing into the stacking direction (*vide supra*) and thus provides the optimal tool to determine the absolute orientation of the *b*-axis. According to the results in Figure 6, maximum PL intensity was observed along the elongated crystal axis (further support came from pronounced optical birefringence, see inset of Figure 3a). Thus, the spectroscopic measurements indeed confirmed that the molecular stack direction along the *b*-axis coincides with the long crystal axis and thus explains the favorable, efficient, and ambipolar charge transport in this direction.

3. CONCLUSION

In conclusion, we have comprehensively investigated the rational design of a mixed stack single-crystalline CT system with efficient red luminescence (Φ_{PL} = 31%) and ambipolar quasi-1D charge-transport properties (μ_h up to 6.7×10^{-3} cm^2 V^{-1} s^{-1} and μ_e up to 6.7×10^{-2} cm^2 V^{-1} s^{-1}). To this end, an isometric **D** and **A** pair with appropriately tuned FMOs was successfully designed and synthesized; DSB- and DCS-based **D** and **A** molecules, respectively.

Our combined in-depth structural, electric, spectroscopic, and computational analysis allowed for a full exploration of all relevant structure−property relationships in this unique system, which can be summarized as follows:

(1) The molecules could be self-assembled into a 1:1 **D**−**A** mixed columnar structure driven by the tailor-made electronic and geometric properties of **D** and **A**, i.e., isometric geometry, favorable Coulomb and H-bonding interactions, and the requirements for electroneutrality and enthalpic arguments.

(2) The lowest excited state in the **D**−**A** (1:1) CT cocrystal is mainly ascribed by a HOMO→LUMO excitation,

dx.doi.org/10.1021/ja312197b | J. Am. Chem. Soc. XXXX, XXX, XXX−XXX

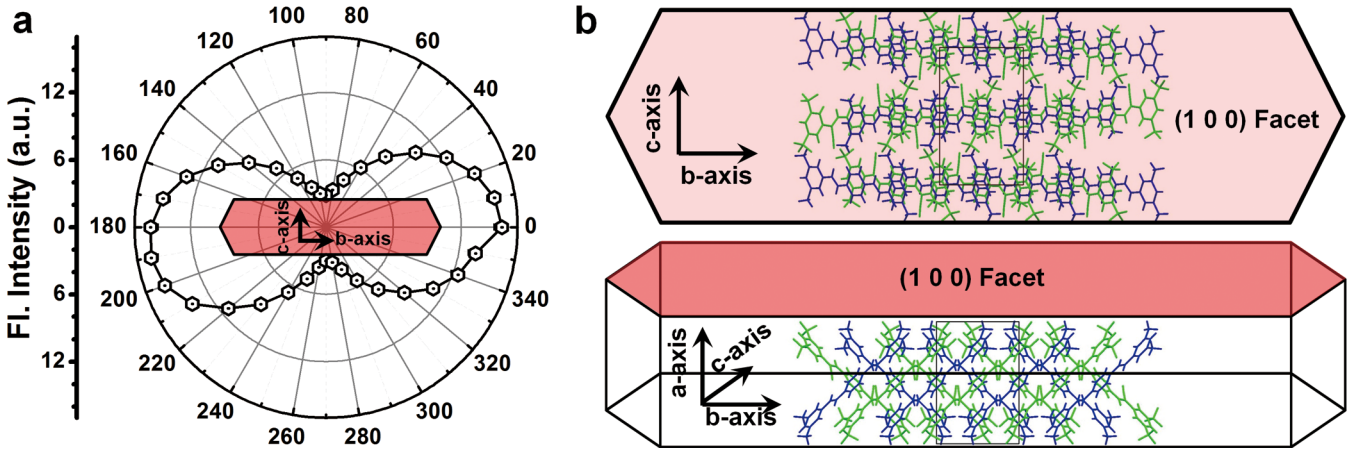

Figure 6. (a) measured PL intensity anisotropy of the **D**−**A** (1:1) CT cocrystal. (b) Schematic drawings of the molecular packing structure with respect to the macroscopic crystal morphology; crystallographic axes are indicated.

where the HOMO and LUMO are entirely localized on the **D** and **A** moiety, respectively. The distinct CT character of the transition gives rise to a strong red-shifted absorption band with moderately small oscillator strength which allows for bright and highly polarized red emission.

(3) Solution-processed single-crystalline OFETs show efficient anisotropic and ambipolar charge carrier transport behavior, with hole and electron mobilities up to 6.7×10^{-3} and 6.7×10^{-2} cm^2 V^{-1} s^{-1}. The transport was proven to occur along the direction of **D**−**A**−**D**−**A** mixed stacks promoted by the densely packed, planar molecules with localized FMOs, which follows a superexchange mechanism to give rise to high p- and n-channel behavior.

Summing up the remarkable properties of the investigated system, our isometric **D**−**A** approach opens a new and versatile route toward highly efficient ambipolar and at the same time bright luminescent materials, which holds important implications for next-generation (opto-)electronic applications.

4. EXPERIMENTAL SECTION

Synthesis and Characterization. 1,4-bis(3,5-dimethylstyryl)-benzene, 4M-DSB, was synthesized by a two-step procedure, as detailed in the SI. (2*Z*,2′*Z*)-3,3′-(1,4-phenylene)bis(2-(3,5-bis-(trifluoromethyl)phenyl)acrylonitrile), CN-TFPA, was synthesized by Knoevenagel condensation, as previously reported.[21]

Sample Preparation. The **D**−**A** (1:1) NP suspension (5×10^{-6} mol L^{-1}) was obtained by reprecipitation from THF:water (1:9, v:v). For this, **D** and **A** were dissolved in THF in 1:1 molar ratio, then distilled water was slowly injected as a poor solvent, left for 2 h before the optical studies, see Figures S11 and S12. Pure **D** and **A** NP suspensions were prepared accordingly. Single-crystalline bulk **D**−**A** (1:1) CT cocrystals were prepared by solvent diffusion from a 1:1 mixture in DCM/methanol.

Structure Analysis. Single-crystal structure analysis was done with a SMART-APEX II ULTRA (Bruker). Out-of-plane XRD measurements were performed using PANalytical X'pert PRO system with a Bragg−Brentano geometry using CuK radiation with a graphite monochromator on the secondary side.

General Characterization. ^{1}H NMR was recorded using a Bruker, Avance-300 (300 MHz) in $CDCl_3$ solution for all materials. ^{13}C NMR was recorded in $CDCl_3$ on a Bruker Avance-500 (500 MHz). Elemental analyses were conducted with a EA1110 (CE Instruments). Mass spectra were measured using a JEOL, JMS-600W spectrometer. UV−vis absorption spectra were done with a Shimazu UV-1650 PC spectrometer. PL spectra were measured using a Varian, Cary Eclipse spectrophotometer. PL spectra on **D**−**A** (1:1) CT cocrystals were recorded using an Anton SP2500 series spectrometer equipped with a nitrogen-cooled CCD camera and with 300 line/mm grating; the spectra were recorded with minimized self-absorption by proper crystal adjustment. Polarized measurements were done with a Glan−Thompson polarizer for the incident laser (405 nm); the analyzer was varied in intervals of 10°. The Φ_{PL} was measured in an integrating sphere (Hamamatsu C9920−01). AFM measurements were carried out in the Nanowizard scanning probe microscope (version 1.3) of JPK instruments, and the images were obtained in the contact mode using a soft cantilever.

Theoretical Quantum Chemical Calculation Methods. Ground-state geometries and MOs of the **D** and **A** compounds were calculated by DFT, imposing C_{2h} symmetry. Vertical EAs and IPs were done on the radical anions and cations based on the neutral geometry, using DCM as a solvent as described by the polarizable continuum model; adiabatic IPs and EAs were obtained on optimized geometries of the radical ions. Excited states of the single molecular species were calculated at the TD-DFT level of theory. For all single molecules the B3LYP functional and 6-311G* basis set were employed as defined in the Gaussian09 program package.[28] **D**−**A** dimer and trimer calculations were done by taking the intermolecular coordinates from X-ray analysis, replacing the molecules by the DFT-optimized ones. Single point (TD-)DFT calculations employed the Coulomb-attenuated method (CAM) variant of the B3LYP functional[29] as implemented in Gaussian09 to correctly account for long-range interactions. The orbital topologies were plotted with Molekel.[30]

Device Fabrication and Measurement. For substrates preparation, SiO_2/Si substrates (p-doped 300 nm) were rinsed with acetone and isopropyl alcohol, respectively, for 10 min in an ultrasonicator, followed by 15 min UV (360 nm) O_3 treatment. **D**, **A** compounds and PMMA (average M_w ∼15 000) were dissolved in 1,2-dichloroethane (0.5 wt % of PMMA, 0.1 wt % of **A** and **D**, 1:1). The solution was spin-coated at 2500 rpm for 1 min. For the SVA process, 4 mL of DCM were injected in 8 mL vial and covered with an as-casted film for 30 min to ensure full growth of the cocrystal. For the top-contact SC-OFETs, 50 nm of Au were thermally deposited through a metal mask in a vacuum chamber. The *I*−*V* characteristics of six individual devices were measured using a Keithley 4200 SCS. All procedures were carried out in a N_2-filled glovebox.

■ ASSOCIATED CONTENT

Ⓢ Supporting Information

Synthesis and characterization, crystallographic information, quantum chemical calculation methods and results, experimental and calculated Raman spectra, capacitance value, AFM, field emission SEM, experimental methods, crystallographic

dx.doi.org/10.1021/ja312197b | J. Am. Chem. Soc. XXXX, XXX, XXX−XXX

data (CIF file, CCDC 905525). CCDC 905525 contains the supplementary crystallographic data for this paper. This data can be obtained free of charge via www.ccdc.cam.ac.uk/data_request/cif or by emailing data_request@ccdc.cam.ac.uk or contacting The Cambridge Crystallographic Data Centre, 12, Union Road, Cambridge CB2 1EZ, UK; fax: +44 1223 336033. This material is available free of charge via the Internet at http://pubs.acs.org.

AUTHOR INFORMATION

Corresponding Author

parksy@snu.ac.kr; johannes.gierschner@imdea.org

Notes

The authors declare no competing financial interest.

ACKNOWLEDGMENTS

This research was supported by Basic Science Research Program (CRI; RIAMI-AM0209(0417-20090011)) and World Class University (WCU) project (R31-2008-000-10075-0) through National Research Foundation of Korea funded by the Ministry of Education, Science and Technology. The work in Madrid was supported by the 'Ministerio de Economia y Competitividad' (CTQ2011-27317, RyC-2007-01559) and Comunidad de Madrid (S2009/MAT-1726, S2009/PPQ-1533). We thank S. Casado, Madrid, for his assistance with the AFM and R. Wannemacher, Madrid, for the help with the low temperature measurements. S.V. thanks for an Amarout grant of the EC (grant no. 229599).

REFERENCES

(1) Tang, C. W.; Van Slyke, S. A. *Appl. Phys. Lett.* **1987**, *51*, 913.

(2) Yu, G.; Gao, J.; Hummelen, J. C.; Wudl, F.; Heeger, A. J. *Science* **1995**, *270*, 1789.

(3) Sirringhaus, H.; Brown, P. J.; Friend, R. H.; Nielsen, M. M.; Bechgaard, K.; Langeveld-Voss, B. M. W.; Spiering, A. J. H.; Janssen, R. A. J.; Meijer, E. W.; Herwig, P.; de Leeuw, D. M. *Nature* **1999**, *401*, 685.

(4) (a) Liu, Y.-Y.; Song, C.-L.; Zeng, W.-J.; Zhou, K.-G.; Shi, Z.-F.; Ma, C.-B.; Yang, F.; Zhang, H.-L.; Gong, X. *J. Am. Chem. Soc.* **2010**, *132*, 16349. (b) Zhang, Y.; Kim, C.; Lin, J.; Nguyen, T.-Q. *Adv. Funct. Mater.* **2012**, *22*, 97.

(5) (a) Meijer, E. J.; De Leeuw, D. M.; Setayesh, S.; Van Veenendaal, E.; Huisman, B.-H.; Blom, P. W. M.; Hummelen, J. C.; Scherf, U.; Klapwijk, T. M. *Nat. Mater.* **2003**, *2*, 678. (b) Babel, A.; Wind, J. D.; Jenekhe, S. A. *Adv. Funct. Mater.* **2004**, *14*, 891.

(6) Sakamoto, Y.; Suzuki, T.; Kobayashi, M.; Gao, Y.; Fukai, Y.; Inoue, Y.; Sato, F.; Tokito, S. *J. Am. Chem. Soc.* **2004**, *126*, 8138.

(7) (a) Mativetsky, J. M.; Kastler, M.; Savage, R. C.; Gentilini, D.; Palma, M.; Pisula, W.; Müllen, K.; Samorì, P. *Adv. Funct. Mater.* **2009**, *19*, 2486. (b) Yamamoto, Y.; Zhang, G.; Jin, W.; Fukushima, T.; Ishii, N.; Saeki, A.; Seki, S.; Tagawa, S.; Minari, T.; Tsukagoshi, K.; Aida, T. *Proc. Natl. Acad. Sci. U.S.A.* **2009**, *106*, 21051.

(8) Babel, A.; Zhu, Y.; Cheng, K.-F.; Chen, W.-C.; Jenekhe, S. A. *Adv. Funct. Mater.* **2007**, *17*, 2542.

(9) Alves, H.; Molinari, A. S.; Xie, H.; Morpurgo, A. F. *Nat. Mater.* **2008**, *7*, 574.

(10) (a) Zhang, J.; Geng, H.; Virk, T. S.; Zhao, Y.; Tan, J.; Di, C.-a.; Xu, W.; Singh, K.; Hu, W.; Shuai, Z.; Liu, Y.; Zhu, D. *Adv. Mater.* **2012**, *24*, 2603. (b) Wakahara, T.; D'Angelo, P.; Miyazawa, K.; Nemoto, Y.; Ito, O.; Tanigaki, N.; Bradley, D. D. C.; Anthopoulos, T. D. *J. Am. Chem. Soc.* **2012**, *134*, 7204. (c) Jonkheijm, P.; Stutzmann, N.; Chen, Z.; de Leeuw, D. M.; Meijer, E. W.; Schenning, A. P. H. J.; Würthner, F. *J. Am. Chem. Soc.* **2006**, *128*, 9535.

(11) (a) Mori, T. *Chem. Lett.* **2011**, *40*, 428. (b) Hasegawa, T.; Mattenberger, K.; Takeya, J.; Batlogg, B. *Phys. Rev. B* **2004**, *69*, 245115. (c) Takahashi, Y.; Hasegawa, T.; Abe, Y.; Tokura, Y.; Nishimura, K.; Saito, G. *App. Phys. Lett.* **2005**, *86*, 063504. (d) Takahashi, Y.; Hasegawa, T.; Abe, Y.; Tokura, Y.; Saito, G. *App. Phys. Lett.* **2006**, *88*, 073504. (e) Kawasugi, Y.; Yamamoto, H. M.; Tajima, N.; Fukunaga, T.; Tsukagoshi, K.; Kato, R. *Phys. Rev. Lett.* **2009**, *103*, 116801. (f) Kawasugi, Y.; Yamamoto, H. M.; Tajima, N.; Fukunaga, T.; Tsukagoshi, K.; Kato, R. *Phys. Rev. B* **2011**, *84*, 125129. (g) Kimata, M.; Ishihara, T.; Tajima, H. *J. Phys. Soc. Jpn.* **2012**, *81*, 073704. (h) Sakai, M.; Sakuma, H.; Ito, Y.; Saito, A.; Nakamura, M.; Kudo, K. *Phys. Rev. B* **2007**, *76*, 045111. (i) Hinderhofer, A.; Schreiber, F. *ChemPhysChem* **2012**, *13*, 628.

(12) (a) Rao, K. V.; George, S. J. *Chem.—Eur. J.* **2012**, *18*, 14286. (b) Schmidt-Mende, L.; Fechtenkötter, A.; Müllen, K.; Moons, E.; Friend, R. H.; MacKenzie, J. D. *Science* **2001**, *293*, 1119. (c) Percec, V.; Glodde, M.; Bera, T. K.; Miura, Y.; Shiyanovskaya, I.; Singer, K. D.; Balagurusamy, V. S. K.; Heiney, P. A.; Schnell, I.; Rapp, A.; Spiess, H.-W.; Hudson, S. D.; Duan, H. *Nature* **2002**, *419*, 384. (d) Sagade, A. A.; Rao, K. V.; Mogera, U.; George, S. J.; Datta, A.; Kulkarni, G. U. *Adv. Mater.* **2013**, *25*, 559.

(13) (a) Wang, C.; Yin, S.; Chen, S.; Xu, H.; Wang, Z.; Zhang, X. *Angew. Chem.* **2008**, *120*, 9189. (b) Wang, C.; Guo, Y.; Wang, Y.; Xu, H.; Wang, R.; Zhang, X. *Angew. Chem.* **2009**, *121*, 9124. (c) Rao, K. V.; Jayaramulu, K.; Maji, T. K.; George, S. J. *Angew. Chem.* **2010**, *122*, 4314. (d) Dössel, L. F.; Kamm, V.; Howard, I. A.; Laquai, F.; Pisula, W.; Feng, X.; Li, C.; Takase, M.; Kudernac, T.; De Feyter, S.; Müllen, K. *J. Am. Chem. Soc.* **2012**, *134*, 5876.

(14) (a) Ferraris, J. P.; Poehler, T. O.; Bloch, A. N.; Cowan, D. O. *Tetrahedron Lett.* **1973**, *14*, 2553. (b) Jérome, D.; Mazaud, A.; Ribault, M.; Bechgaard, K. *J. Phys., Lett.* **1980**, *41*, L95. (c) Batail, P. *Chem. Rev.* **2004**, *104*, 4887.

(15) Tayi, A. S.; Shveyd, A. K.; Sue, A. C.-H.; Szarko, J. M.; Rolczynski, B. S.; Cao, D.; Kennedy, T. J.; Sarjeant, A. A.; Stern, C. L.; Paxton, W. F.; Wu, W.; Dey, S. K.; Fahrenbach, A. C.; Guest, J. R.; Mohseni, H.; Chen, L. X.; Wang, K. L.; Stoddart, J. F.; Stupp, S. I. *Nature* **2012**, *488*, 485.

(16) Zhu, L.; Yi, Y.; Li, Y.; Kim, E.-G.; Coropceanu, V.; Brédas, J.-L. *J. Am. Chem. Soc.* **2012**, *134*, 2340.

(17) Döttinger, S. E.; Hohloch, M.; Segura, J. L.; Steinhuher, E.; Hanack, M.; Tompert, A.; Oelkrug, D. *Adv. Mater.* **1997**, *9*, 233.

(18) (a) An, B.-K.; Gierschner, J.; Park, S. Y. *Acc. Chem. Res.* **2012**, *45*, 544. (b) Yoon, S.-J.; Chung, J. W.; Gierschner, J.; Kim, K. S.; Choi, M.-G.; Kim, D.; Park, S. Y. *J. Am. Chem. Soc.* **2010**, *132*, 13675.

(19) Gierschner, J.; Ehni, M.; Egelfaaf, H.-J.; Medina, B. M.; Beljonne, D.; Benmansour, H.; Bazan, G. C. *J. Chem. Phys.* **2005**, *123*, 144914.

(20) Bartholomew, G. P.; Bu, X.; Bazan, G. C. *Chem. Mater.* **2000**, *12*, 2311.

(21) Park, S. K.; Kim, J. H.; Yoon, S.-J.; Kwon, O. K.; An, B.-K.; Park, S. Y. *Chem. Mater.* **2012**, *24*, 3263.

(22) (a) Lee, W. H.; Lim, J. A.; Kwak, D.; Cho, J. H.; Lee, H. S.; Choi, H. H.; Cho, K. *Adv. Mater.* **2009**, *21*, 4243. (b) Liu, C.; Minari, T.; Lu, X.; Kumatani, A.; Takimiya, K.; Tsukagoshi, K. *Adv. Mater.* **2011**, *23*, 523.

(23) An, B.-K.; Kwon, S.-K.; Jung, S.-D.; Park, S. Y. *J. Am. Chem. Soc.* **2002**, *124*, 14410.

(24) Kabe, R.; Nakanotani, H.; Sakanoue, T.; Yahiro, M.; Adachi, C. *Adv. Mater.* **2009**, *21*, 4034.

(25) Gierschner, J.; Mack, H.-G.; Oelkrug, D.; Waldner, I.; Rau, H. *J. Phys. Chem. A* **2004**, *108*, 257.

(26) (a) Coropceanu, V.; Cornil, J.; da Silva Filho, D. A.; Olivier, Y.; Silbey, R.; Brédas, J.-L. *Chem. Rev.* **2007**, *107*, 926. (b) Giri, G.; Verploegen, E.; Mannsfeld, S. C. B.; Atahan-Evrenk, S.; Kim, D. H.; Lee, S. Y.; Becerril, H. A.; Aspuru-Guzik, A.; Toney, M. F.; Bao, Z. *Nature* **2011**, *480*, 504.

(27) Zaumseil, J.; Sirringhaus, H. *Chem. Rev.* **2007**, *107*, 1296.

(28) Frisch, M. J.; Trucks, G. W.; Schlegel, H. B.; Scuseria, G. E.; Robb, M. A.; Cheeseman, J. R.; Scalmani, G.; Barone, V.; Mennucci, B.; Petersson, G. A.; Nakatsuji, H.; Caricato, M.; Li, X.; Hratchian, H. P.; Izmaylov, A. F.; Bloino, J.; Zheng, G.; Sonnenberg, J. L.; Hada, M.; Ehara, M.; Toyota, K.; Fukuda, R.; Hasegawa, J.; Ishida, M.; Nakajima,

T.; Honda, Y.; Kitao, O.; Nakai, H.; Vreven, T.; Montgomery, J. A., Jr.; Peralta, J. E.; Ogliaro, F.; Bearpark, M.; Heyd, J. J.; Brothers, E.; Kudin, K. N.; Staroverov, V. N.; Kobayashi, R.; Normand, J.; Raghavachari, K.; Rendell, A.; Burant, J. C.; Iyengar, S. S.; Tomasi, J.; Cossi, M.; Rega, N.; Millam, J. M.; Klene, M.; Knox, J. E.; Cross, J. B.; Bakken, V.; Adamo, C.; Jaramillo, J.; Gomperts, R.; Stratmann, R. E.; Yazyev, O.; Austin, A. J.; Cammi, R.; Pomelli, C.; Ochterski, J. W.; Martin, R. L.; Morokuma, K.; Zakrzewski, V. G.; Voth, G. A.; Salvador, P.; Dannenberg, J. J.; Dapprich, S.; Daniels, A. D.; Farkas, Ö.; Foresman, J. B.; Ortiz, J. V.; Cioslowski, J.; Fox, D. J. *Gaussian 09*, revision A.02; Gaussian, Inc.: Wallingford, CT, 2009.

(29) Yanai, T.; Tew, D. P.; Handy, N. C. *Chem. Phys. Lett.* **2004**, *393*, 51.

(30) Flukiger, P.; Luthi, H. P.; Portmann, S.; Weber, J. *MOLEKEL*, version 4.3; Swiss National Computing Centre CSCS: Manno, Switzerland, 2000; http://www.cscs.ch/molkel/.